

## SUPPLEMENTARY MATERIAL: The Effect of Pyrolysis on Pitch Chemical, Thermal and Rheological Properties

### Authors

Heedong Yoon<sup>1</sup>, Zachary R. Hinton<sup>1</sup>, James Heinzman<sup>1</sup>, Clarence E. Chase<sup>2</sup>, Manesh Gopinadhan<sup>2</sup>, Kazem V. Edmond<sup>2</sup>, Daniel J. Ryan<sup>3</sup>, Stuart E. Smith<sup>2</sup>, and Nicolas J. Alvarez<sup>1\*</sup>

### Affiliations

1. Chemical and Biological Engineering Department, Drexel University, 3141 Chestnut St., Philadelphia, PA, 19104, USA

2. Corporate Strategic Research, ExxonMobil Research and Engineering Company, 1545 Route 22 E., Annandale, NJ, 08801, USA

3. Analytical Sciences Laboratory, ExxonMobil Research and Engineering Company, 1545 Route 22 E., Annandale, NJ, 08801, USA

## 1. Analysis

### 1.1 Z-number

The Z-number is an indicator of hydrogen deficiency and is expressed according to the following representative molecular structure:  $C_cH_{2c+Z}N_nS_sO_o$ , where c, n, s, and o represents the number of carbon, nitrogen, sulfur and oxygen atoms, respectively. Homologous series of an aromatic core and heteroatom combination will have one unique Z-number. Plotting Z-number and carbon number provides greater compositional information than  $m/z$  plots alone and allows for a direct measure of the aromaticity of the pitch components.

### 1.2 Shear Rheology

The modulus determined from multimode (n) Maxwell model is defined by

$$G(t) = \sum_1^n g_i e^{-t/\tau_i} \quad (1)$$

where  $g_i$  and  $\tau_i$  are modulus and relaxation time at each mode.<sup>43, 47</sup>

Then, zero shear viscosity ( $\eta_0$ ) can be calculated by following equation.<sup>43, 47</sup>

$$\eta_0 = \sum_1^n g_i \tau_i \quad (2)$$

The WLF equation<sup>78</sup> is defined by

$$\log_{a_T} = \left( \frac{\tau}{\tau_R} \right) = \frac{-C_1(T-T_R)}{C_2+T-T_R} \quad (3)$$

where  $\tau$  is the relaxation time and  $C_1$  and  $C_2$  are constant.

### 1.3 Extensional Rheology

The ‘Hencky strain’ ( $\varepsilon_{D(t)}$ ) and ‘Axial Hencky strain( $\varepsilon_{z(t)}$ )’ represent the measured diameter and the length of the fibers at a specific time during the stretching process.  $\varepsilon_{D(t)}$  and  $\varepsilon_{z(t)}$  are the essential parameters for fiber spinning, which give the information on obtaining critical length and diameter to produce continuous filament structures in the melt spinning process. The ‘Hencky strain’ ( $\varepsilon_{D(t)}$ ) is calculated using the following equations.<sup>47, 48</sup>

$$\varepsilon_D (t) = -2\ln \left( \frac{R(t)}{R_0} \right) \quad (4)$$

where  $R(t)$  is the radius of the filament mid-point and  $R_0$  is the radius of a molded sample. In the case of ‘Axial Hencky strain’ ( $\varepsilon(t)$ ):

$$\varepsilon_A (t) = \ln \left( \frac{L(t)}{L_0} \right) \quad (5)$$

where  $L(t)$  is the length of the filament and  $L_0$  is the height of a molded sample. Stress acting on the filament is defined by:

$$\sigma (t) = \frac{F(t)-m_f g/2}{\pi R(t)^2} \times \frac{1}{\left(1+\left(\frac{R(t)}{R_0}\right)^{\frac{10}{3}}\right) \times \exp\left(\frac{-\Lambda_0^3}{3\Lambda_0^2}\right)} \quad (6)$$

where  $F(t)$  is force measured by the VADER 1000,  $m_f$  is weight of the filament,  $g$  is the gravitational acceleration, and  $A_0$  is aspect ratio ( $R_0/L_0$ ) of the sample.<sup>47, 48</sup> Stress growth coefficient ( $\eta^+$ ) is defined by  $\sigma(t)/\dot{\epsilon}(t)$  where  $\dot{\epsilon}(t)$  is  $\epsilon(t)/dt$ .<sup>47, 48</sup>

$\tau_i$ [s]	$g_i$ [Pa]
4.28E+07	2.67E+00
1.27E+07	1.25E+00
3.77E+06	2.21E+00
1.12E+06	4.23E+00
3.32E+05	7.53E+00
9.86E+04	1.56E+01
2.93E+04	3.80E+01
8.69E+03	5.76E+01
2.58E+03	4.95E+02
7.65E+02	3.07E+03
2.27E+02	2.04E+04
6.74E+01	1.17E+05
2.00E+01	6.77E+05
5.94E+00	9.96E+06
1.76E+00	4.29E+07
5.24E-01	6.75E+07
1.55E-01	3.02E+07
4.61E-02	2.99E+07
1.37E-02	3.96E+07
4.07E-03	2.51E+07

**Table S1.** Maxwell units used for the curve fitting in Fig. 5a.

## 2. Results and Discussions

### 2.1 Z Analysis for Mass Spectra

From the high-resolution MS data, molecular formulas can be assigned for each peak, permitting the calculation of the Z-number for the molecule. The Z-number is an indicator of hydrogen deficiency and is expressed according to the following representative molecular structure:  $C_cH_{2c+Z}N_nS_sO_o$ , where c, n, s, and o represents the number of carbon, nitrogen, sulfur and oxygen atoms, respectively. Homologous series of an aromatic core and heteroatom combination will have one unique Z-number. Plotting Z-number and carbon number provides greater compositional information than  $m/z$  plots alone and allows for a direct measure of the aromaticity of the pitch components. Figure S1 shows a fractional species plot of the four most abundant species, i.e. hydrocarbon (HC), nitrogen (1N), oxygen (1O and 2O). Note that the number indicates the number of heteroatoms present within the molecule. Figure S2 highlights the change in Z class between the 3 samples by plotting the total summed intensity for a given Z class for all of the hydrocarbon species.

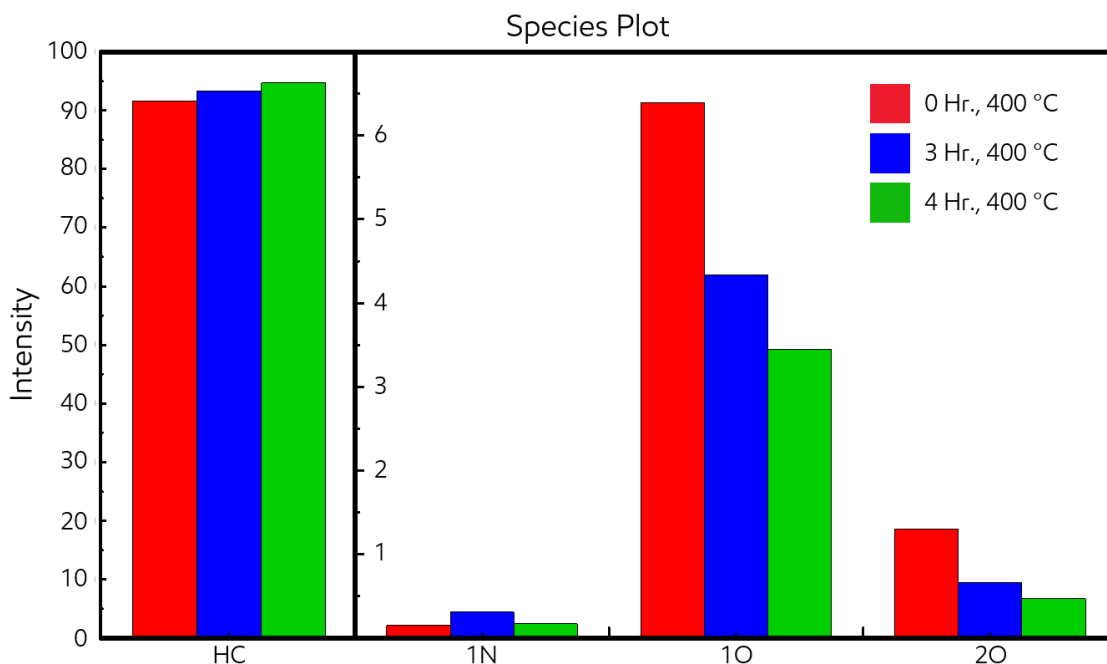


**Figure S1.** A species plot highlighting the most abundant molecular classes detected from the FT-ICR MS data.

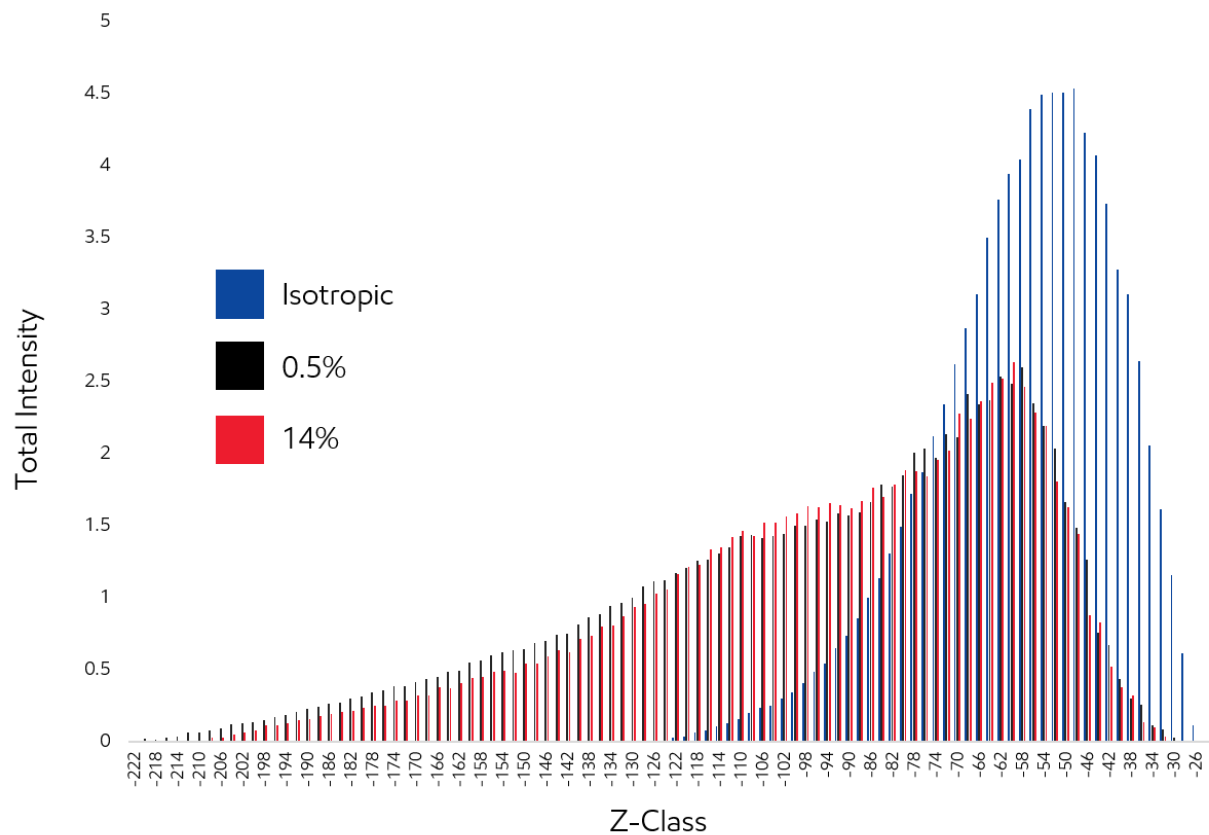


**Figure S2.** The Z-Class distributions are presented using the total intensity for the hydrocarbon (HC) species identified from the 3 pitch samples.

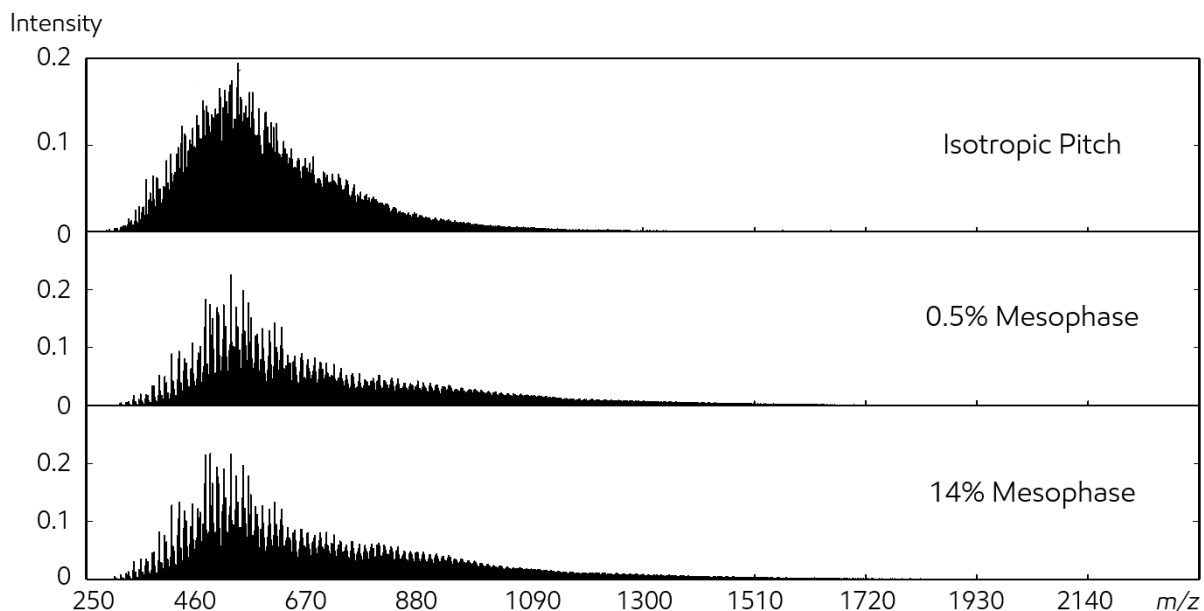


**Figure S3** Average mass spectra for each of the 3 pitch samples acquired on a 15T FT-ICR MS.

## 2.2 Analysis for DSC

Figure S4 shows the DSC heating scans for Iso, Meso 0.5 %, and Meso 14 % pitch samples. In general, the first heating scan in a DSC measurement is performed to erase the material's thermal history. However, the first heating scan also provides material information related to chemical reactions, aging response, and crystallization.<sup>38, 58-61</sup> In particular, it is extensively used to interpret the materials' aging response or thermal history<sup>38, 58, 59</sup> Hence, to also investigate the thermal history of the pitch samples, we compare the first and second heating scan curves.

Figure S4a shows the first heating scans for the isotropic and mesophase pitch samples. Glass transitions were observed for Iso and Meso 0.5 %, denoted by a clear step change ( $\Delta C_p$ )<sup>40</sup> in heat flow between 90 °C and 110 °C. However, the  $T_g$  for Meso 14 %, is preceded by an exothermic transition presumably due to reaction of the pitch with air trapped in the DSC pan. This exothermic

peak was reported in prior studies<sup>62</sup>, which argues that it is due to chemical changes from oxygen trapped in the DSC pan. Figure S4b shows the second heating curves for the isotropic and mesophase pitch samples. Clear heat capacity step changes were observed for all three samples. The second heating scan for Iso and Meso 0.5 % are very similar to the first scan, while the second heating scan for Meso 14 % shows no exothermic peak. Another interesting point is that small endothermic peaks were developed at 40 °C for both first and second heating scans (both isotropic and mesophase pitch). Currently, we do not understand the origin of this peak. The endothermic peaks are generally attributed to the melting of crystalline structures or the aging response of materials.<sup>37, 38, 58-61</sup> However, since the peak only appears in the first heating scans for the latter case, we expect that this is presumably due to the tiny fraction of crystalline aliphatic content. The  $T_g$  of each sample was determined from the second heating scan using the “Moynihan method”<sup>41, 42</sup>. The detailed method for determining  $T_g$  is described elsewhere.<sup>41, 42</sup> The estimated  $T_g$  for Iso, Meso 0.5 %, and Meso 14 % were 99 °C, 105 °C, and 114 °C, respectively. As expected from the FTIR and MS analysis,  $T_g$  increases with decreasing aliphatic content and increasing aromatic content.

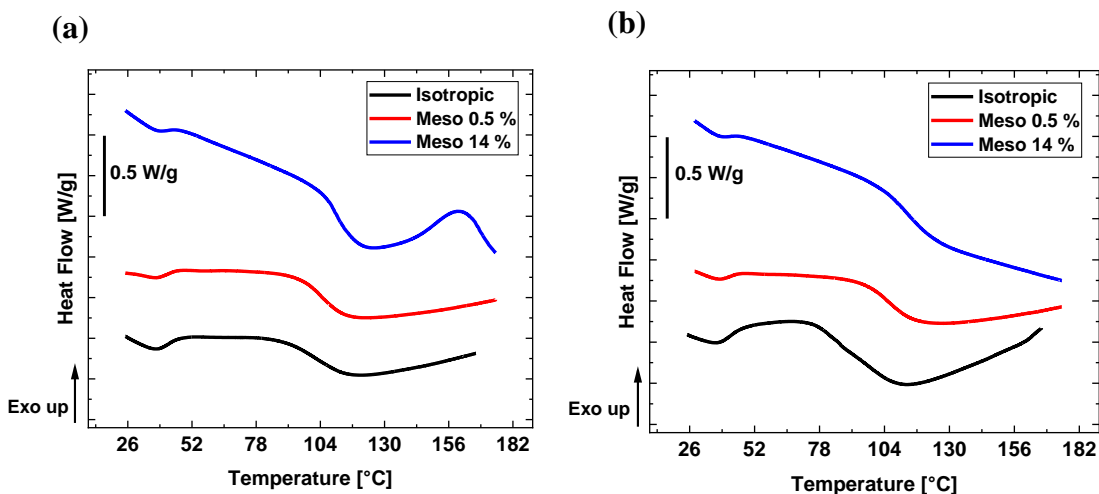


**Figure S4:** DSC heating scans for Iso, Meso 0.5 %, and Meso 14 % pitches. (a) first heating scans. (b) second heating scans.

### 2.3 Thermal Stability of Pitch Samples

Figure S5 shows the weight loss for Iso, Meso 0.5 %, and Meso 14 %, as measured by TGA. An 80% weight loss occurred for Iso when the temperature was increased to 580 °C. In the case of Meso 0.5 %, and Meso 14 %, the weight loss behaviors were almost identical with 50% weight loss at 550 °C. The fact that an increase in mesophase content does not affect the TGA data, and the degree of change in  $M_w$  and Z-class distribution is small suggests that the pitch is approaching a steady state chemical change after 3 h of pyrolysis. Further study is required to better understand the relationship between thermal stability, glass transition temperature, and molecular weight of isotropic pitch during pyrolysis.

Another reason for studying the thermal stability of the material with TGA is to determine whether mass loss is expected at spinning temperature. As mentioned above, spinning is generally performed at temperatures between  $T_s+30$  °C to  $T_s+80$  °C.<sup>1, 10, 15</sup> Figure S5b presents weight loss as a function of  $T-T_s$ . For all samples, there is no significant weight loss at the spinning temperature regime (indicated by the red bar). Furthermore, the current pitch samples do not show any weight loss even at 200 °C above  $T_s$ . Hence, these samples show promise as potential feeds for carbon fiber production since they are able to form filaments and there is minimal volatilization at the high temperature spinning conditions.

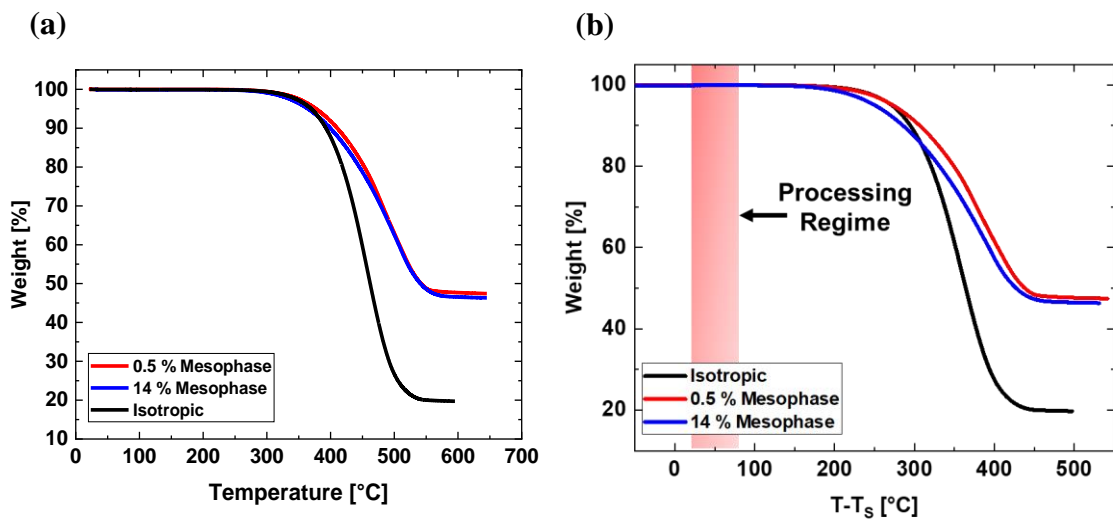


**Figure S5:** Weight loss measured by TGA for Iso, Meso 0.5 %, and Meso 14 % pitch samples.

## 2.4 Shear Rheological Behavior of Pitch

The effect of mesophase on the viscoelastic behavior of isotropic pitch was examined by shear and extensional rheology. We first performed the strain amplitude experiments to determine the linear viscoelastic regime. Figure S6 shows the results of strain amplitude experiments for Meso 0.5 % at a fixed frequency of 1 rad/sec. The experiments were performed at two temperatures that were used for the lowest and highest temperatures in the frequency sweep experiments. At 115 °C, the storage ( $G'$ ) and loss ( $G''$ ) modulus were nearly independent of the strain up to 1 % of strain, and above 1%, the  $G'$  and  $G''$  started to decrease. At 170 °C, the  $G'$  and  $G''$  were independent of the strain up to 10 %. In the current work, 0.6 % of strain was used for the frequency sweep experiments for mesophase pitch samples.

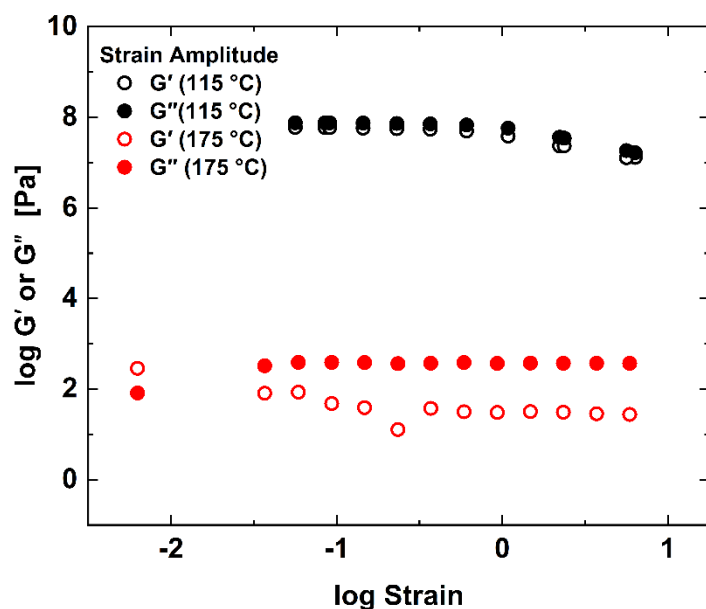


**Figure S6:** Strain amplitude results for Meso 0.5 % sample at 115 °C and 175 °C at a frequency of 1 rad/s.

Figure S7 shows complex viscosity ( $\eta^*$ ) as a function of frequency for Iso, Meso 0.5 % and Meso 14 % determined from the frequency sweep experiments. For Iso at high temperature, we see that  $\eta^*$  is independent of frequency and a very weak function at low temperatures. Similarly, at high temperatures (130~165 °C) Meso 0.5 % shows a very weak dependence of  $\eta^*$  on frequency, i.e. almost Newtonian, but significant shear thinning behavior at lower temperatures (115~125 °C). However, the Meso 14 % shows a strong shear thinning behavior, i.e.  $\eta^*$  continuously decreases with increasing frequency for all temperatures. These results agree with previous studies that indicate Newtonian behavior for isotropic pitch and nonlinear shear thinning rheology for mesophase pitch<sup>25, 26</sup>.

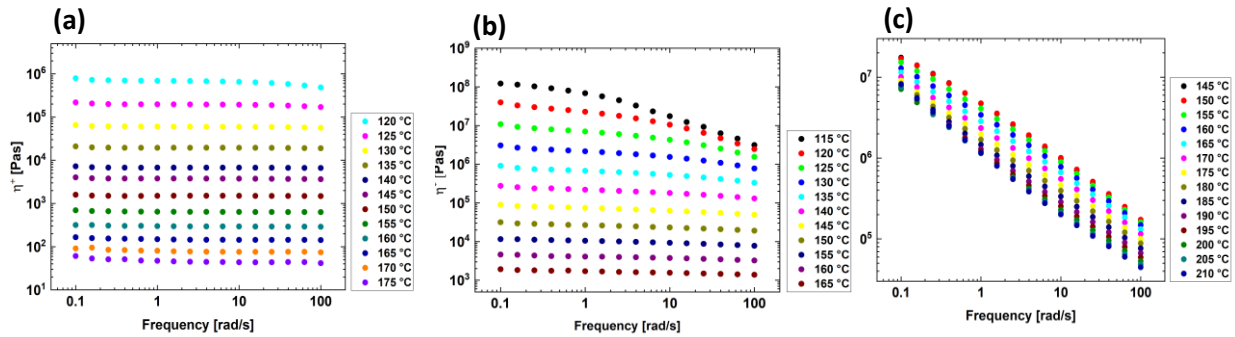


**Figure S7:** Complex viscosities for (a) Iso, (b) Meso 0.5 %, and (c) Meso 14 %.

Figure S8a and b show storage ( $G'$ ) and loss ( $G''$ ) modulus for isotropic pitch measured in the temperature range from 100 °C to 175 °C. In the temperature range from 100 to 135 °C, both  $G'$  and  $G''$  continuously increased with increasing frequency. The increasing rate was weak at high frequency when the temperature was lower than 115 °C. Above 135 °C,  $G'$  modestly increased in the lower frequency regime, then it rapidly increased at higher frequency, whereas  $G''$  continuously increased with increasing frequency. Note that  $G'$  in the glassy regime (higher frequency regime at 110 °C) was lower than expected ( $G' \sim 9$  to 10). This is due to instrument compliance effects discussed in the literature<sup>44, 45</sup>. In any case, this study focuses on the dynamic behavior in the processing regime, which is far above the glass transition temperature. Hence, we did not show the data ( $G'$  or  $G''$ ) above 30MPa, which starts to affect by instrument compliance.

To understand shorter and longer time viscoelastic responses, Time-temperature superposition (TTS) was applied to obtain master curves of  $G'$  and  $G''$ <sup>37, 69, 80</sup>. Before applying TTS, van Gurp-Palmen (vGP) and  $\tan \delta$  plots were first generated to test the validity of TTS.<sup>69, 70</sup> In a vGP plot, TTS is considered applicable if  $\delta$  versus  $G^*$  forms a master curve without additional horizontal shifts.<sup>69, 70</sup> Figure S8c shows the vGP plot obtained from frequency sweep data for isotropic pitch. Although there are some small deviations of the vGP curves in the temperature range, 160 to 175 °C, a master vGP curve is observed for isotropic pitch, which

indicates that TTS is generally applicable from 100 °C to 175 °C. The observed discrepancy at high temperature and high frequency is unclear.  $\delta$  rapidly increases with increasing complex modulus ( $G^*$ ) and reaches a maximum value of 90 and remains constant for  $\log G^* < 6$  GPa, indicating a purely viscous material. At 6 GPa,  $\delta$  rapidly decreases again, indicating a transition into the glassy state. Since TTS is generally applicable in the current isotropic pitch sample, shift factors were determined from shifts of  $\tan \delta$  as shown in Figure S8d.

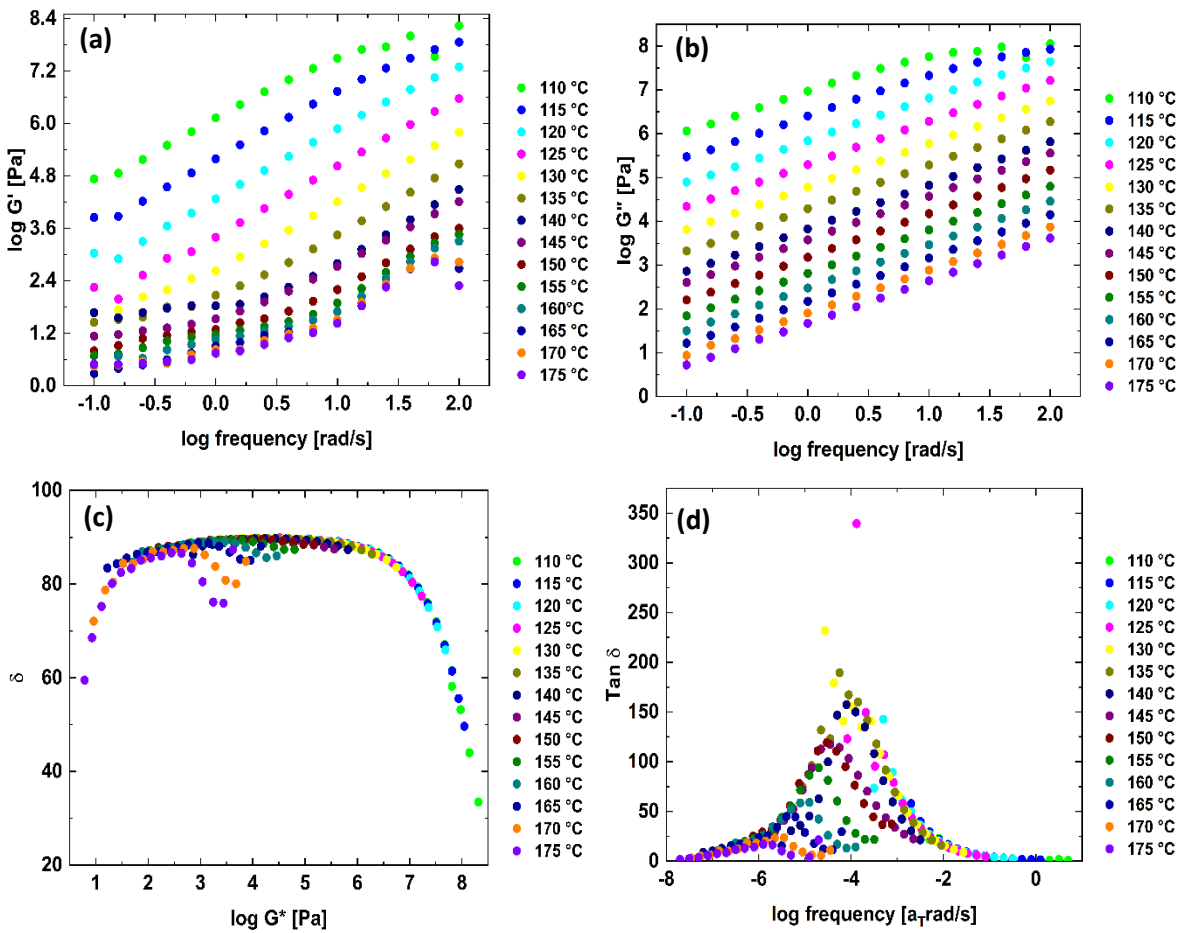


**Figure S8:** Rheological properties for isotropic pitch samples measured in the temperature range from  $T_g + 2$  °C to  $T_g + 67$  °C. (a)  $G'$ , (b)  $G''$ , (c)  $\tan \delta$  and (d) vGP plot.

## 2.5 Extensional Rheological Behavior of Pitch

Figure S9a shows the measured force for isotropic pitch with different strain rates measured at 150 °C. In Figure S9a, we see that the force decreased with increasing strain. Also, the force-strain curves show typical increasing force response with applying a strain rate. The red dashed line (0.1g) is the limit of the current force transducers, which we see that the forces eventually reached to the instrument limit with increasing strain. Since the data obtained below the instrument limit are scattered, which might give wrong interpretation and information for the analysis, we eliminated the data beyond this regime (0.1g). Figure S9b-d show the measured force for Iso, Meso 0.5 %, and Meso 14 % at a different temperature and a fixed strain rate of 1 s<sup>-1</sup>. Like the 150 °C measurement, the force measured at all temperatures for isotropic and mesophase pitch decreased with increasing strain. We also see that the force increased with decreasing temperature at a given strain. Unlike Iso and Meso 0.5 % pitch, the measured forces for the Meso 14 % were well above the instrument limit for all temperatures and strains investigated.

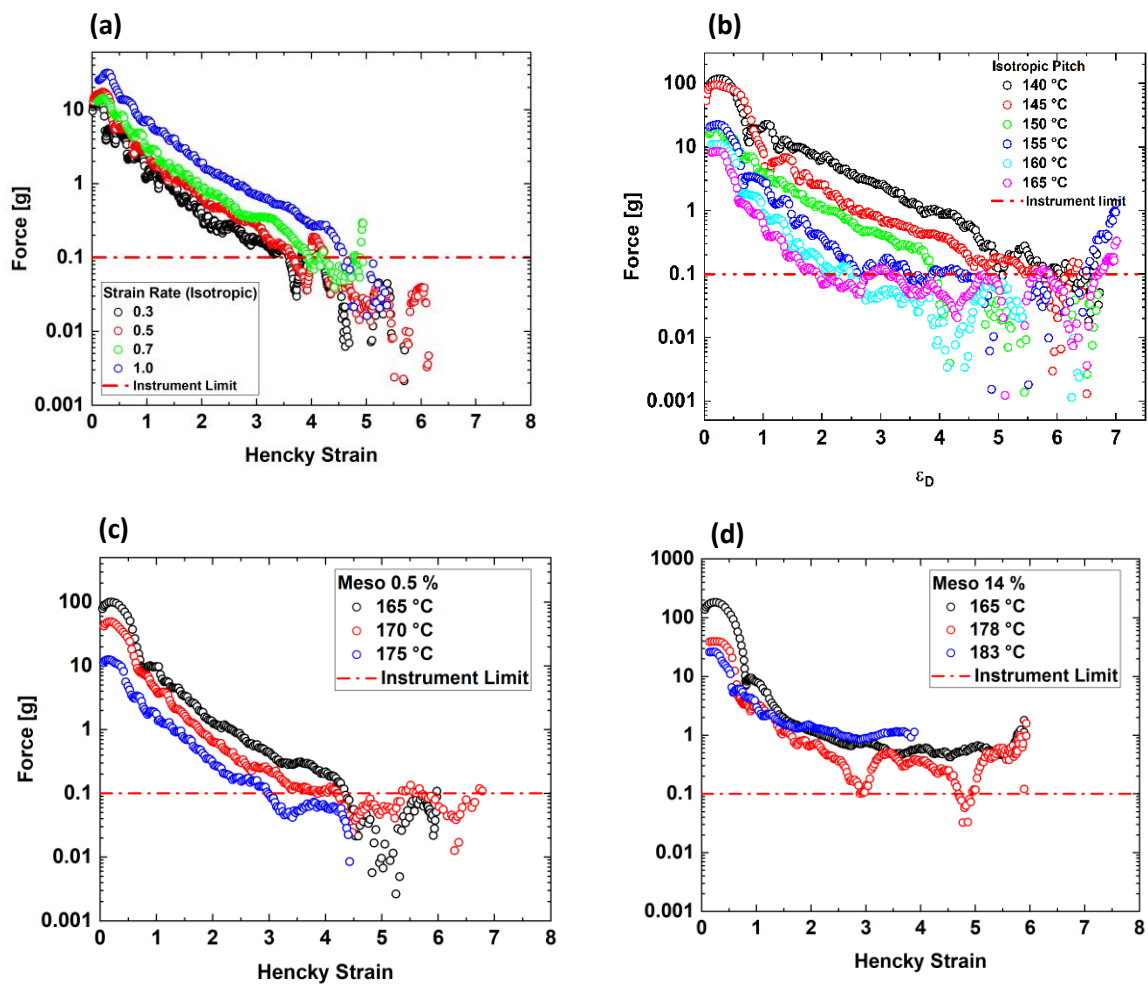


**Figure S9.** Force profile measurements. (a) Iso pitch with different strain rates at 150 °C, (b) Iso pitch at varying temperatures and a fixed strain rate of 1 s<sup>-1</sup>, (c) Meso 0.5 % pitch at varying temperatures and a fixed strain rate of 1 s<sup>-1</sup>, and (d) Meso 14 % mesophase pitch at varying temperatures and a fixed strain rate of 1 s<sup>-1</sup>.

## 2.6 Reproducibility Experiments for Pitch

Figure S10 shows the reproducibility results from shear and extensional rheological measurements for Iso, Meso 0.5 %, Meso 14 % samples. The measurements were performed two to three runs for each sample. Figure 10 a, b, c show the  $G'$  and  $G''$  master curves obtained after applying TTS for Iso, Meso 0.5 %, Meso 14 % samples. For the shear rheological measurements, though there are some small deviations, the results showed good reproducibility. In contrast, the results were more sensitive about the sample heterogeneity for the extensional rheology, where we see the different viscosity profiles for each run in the Meso 14 % sample. This was more clearly seen in Figure 6 that the  $\eta^+$  for the Meso 14 % sample was significantly lower than the LVE.

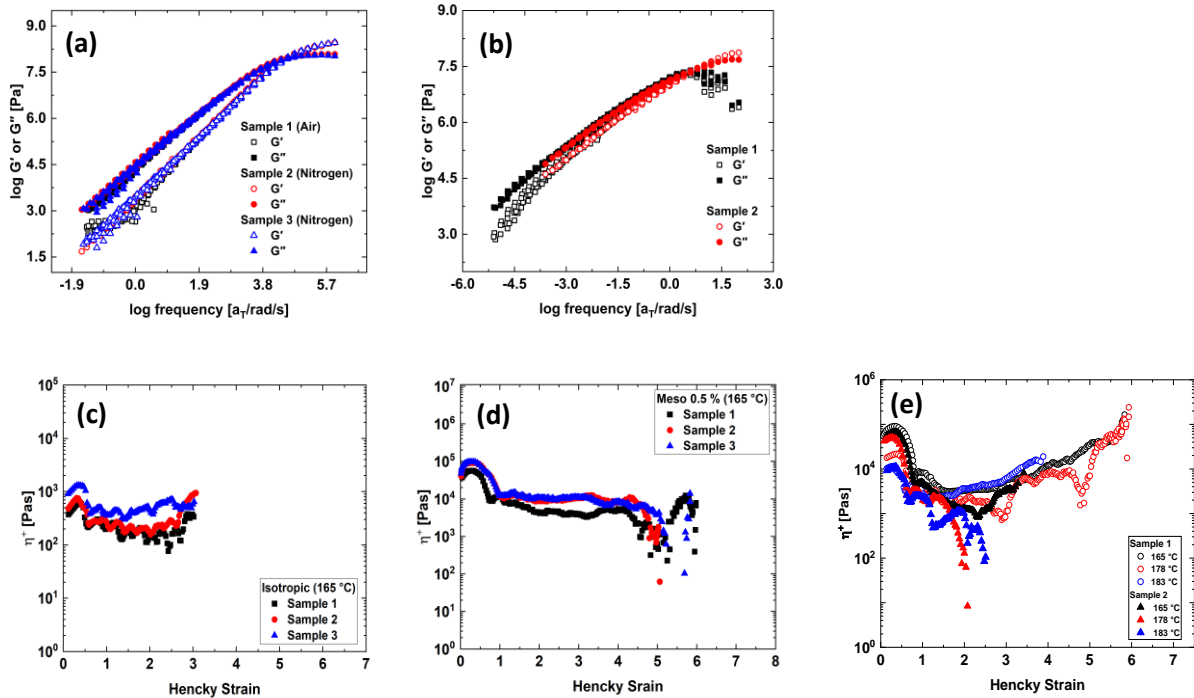


**Figure S10.** Reproducibility experiments for Iso, Meso 0.5 % and Meso 14 %. The rheological properties were measured in different positions of sample batches. Reduced storage and loss modulus obtained from frequency sweep experiments after applying time temperature superposition for (a) Meso 0.5 % and (b) Meso 14 % samples.  $\eta^+$  measured at 165 °C for (c) Iso, (d) Meso 0.5 %, and (e) Meso 14 %.